Observation of the Eckhaus Instability in Whispering-Gallery Mode Resonators

Damià Gomila[1],*, Pedro Parra-Rivas[2,3], Pere Colet[1], Aurélien Coillet[4,5], Guoping Lin[4,6],
Thomas Daugey[4], Souleymane Diallo[4], Jean-Marc Merolla[4], and Yanne K. Chembo[4,7]†

[1]*Instituto de Física Interdisciplinar y Sistemas Complejos, IFISC (CSIC-UIB),
Campus Universitat de les Illes Balears, E-07122 Palma de Mallorca, Spain*
[2]*Laboratory of Dynamics in Biological Systems, KU Leuven Department of
Cellular and Molecular Medicine, University of Leuven, B-3000 Leuven, Belgium*
[3]*Service OPERA-photonique, Universite libre de Bruxelles (ULB),
50 Avenue F. D. Roosevelt, CP194/5 B-1050 Bruxelles, Belgium*
[4]*FEMTO-ST Institute, Univ. Bourgogne Franche-Comté, CNRS,
15B Avenue des Montboucons, 25030 Besançon cedex, France*
[5]*Laboratoire Interdisciplinaire Carnot de Bourgogne,
Univ. Bourgogne-Franche-Comté, CNRS, 9 Avenue A. Savary, 21078 Dijon, France*
[6]*MOE Key Laboratory of Fundamental Quantities Measurement, School of Physics,
Huazhong University of Science and Technology, Wuhan 430074, China*
[7]*University of Maryland, Department of Electrical and Computer Engineering,
& Institute for Research in Electronics and Applied Physics (IREAP)
8279 Paint Branch Dr, College Park MD 20742, USA*
(Dated: February 6, 2020)

The Eckhaus instability is a secondary instability of nonlinear spatiotemporal patterns in which high-wavenumber periodic solutions become unstable against small-wavenumber perturbations. We show in this letter that this instability can take place in Kerr combs generated with ultra-high Q whispering-gallery mode resonators. In our experiment, sub-critical Turing patterns (rolls) undergo Eckhaus instabilities upon changes in the laser detuning leading to cracking patterns with long-lived transients. In the spectral domain, this results in a metastable Kerr comb dynamics with a timescale that can be larger than one minute. This ultra-slow timescale is at least seven orders of magnitude larger than the intracavity photon lifetime, and is in sharp contrast with all the transient behaviors reported so far in cavity nonlinear optics, that are typically only few photon lifetimes long (i. e., in the ps to μs range). We show that this phenomenology is well explained by the Lugiato-Lefever model, as the result of an Eckhaus instability. Our theoretical analysis is found to be in excellent agreement with the experimental measurements.

PACS numbers:

Kerr optical frequency combs are obtained through pumping a high-Q whispering-gallery mode (WGM) cavity with a resonant laser [1]. In the last decade, the experimental and theoretical study of these combs has permitted major advances in photonics (see review articles [2–5]). From the applications standpoint, Kerr combs have been developed for time-frequency metrology, ultra-stable microwave generation, spectroscopy, and optical communications, just to name a few. From the fundamental perspective, Kerr combs have provided an ideal platform to investigate light-matter interactions in confined media. It has been shown that a wide variety of dissipative structures could be excited in the WGM resonators, being either stationary (azimuthal roll patterns, cavity solitons, platicons) or non-stationary (breather solitons, spatiotemporal chaos, rogue waves). The primary bifurcations leading to these various patterns have also been the focus of a detailed analysis in the literature [6–13]. However, only a limited attention has been also devoted to secondary bifurcations, which lead to the destabilization of the stationary patterns [13, 15–17].

In this letter, we evidence experimentally one of these secondary bifurcations in 1D, namely the Eckhaus in-

stability, which emerges when a roll (or stripes) pattern looses its stability against small-wavenumber perturbations. The Eckhaus instability has long been studied in fluid mechanics [21, 22], liquid crystals [23], nonlinear optics [13, 15, 24–26], or systems with delayed feedback [27]. Experimental observations are however much more lim-
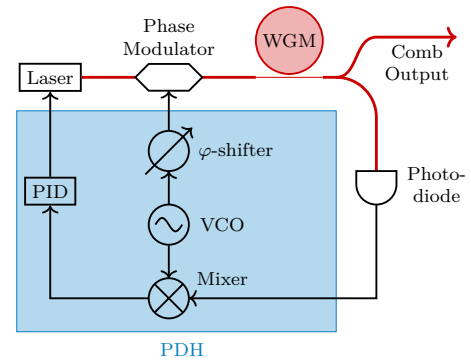

FIG. 1: (Color online) Experimental setup. PID: Proportional-integral-derivative controller; VCO: Voltage-controlled oscillator; PDH: Pound-Drever-Hall locking scheme; WGM: Whispering-gallery mode resonator.
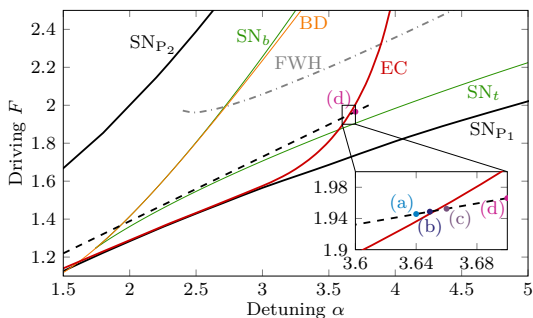
FIG. 2: (Color online) Bifurcation lines of the homogeneous solutions and the roll pattern with $L = 55$ in the parameter space (α, F). The HSS is stable below the MI line for $\alpha < 2$ and below the SN_b line for $\alpha > 2$. The pattern is stable above the Eckhaus line (EC) and below the SN_{P_2} or FWH line, whichever comes first. The dashed line shows the ramp of parameters applied to the pattern, starting from $(\alpha, F) = (1, 1.05)$ to $(3.8, 2)$ beyond the Eckhaus instability.

ited since large aspect-ratio patterns are required, while being difficult to attain in most systems. The Eckhaus instability can also be induced by spatial inhomogeneities [25, 28], an effect that has been observed experimentally in a liquid crystal layer with optical feedback [24]. Other secondary instabilities and parametric perturbations may also hinder Eckhaus instabilities [22, 23]. Counterintuitively, despite their relatively small size, WGM resonators can output large aspect-ratio roll patterns with tens or even hundreds of peaks [29], making the system more susceptible to develop small-wavenumber (or long-wavelength) instabilities.

Our experimental system is displayed in Fig. 1. A MgF_2 WGM resonator with intrinsic quality factor $Q_{in} = 1.8 \times 10^9$ is pumped by a resonant laser at 1552 nm. The resonator has a diameter $d \simeq 11.8$ mm and group-velocity refraction index $n_g = 1.37$, yielding a free-spectral range $FSR = c/n_g \pi d \simeq 5.9$ GHz, where c is the velocity of light in vacuum. When the resonator is pumped above threshold, roll patterns emerging from a Turing or modulational instability (MI) can be excited inside the cavity. They are characterized by an integer number of azimuthal rolls fitting the inner periphery of the disk. The integer number L of rolls (or "peaks") in the azimuthal direction is the wavenumber of the pattern, and in the spectral domain, these roll patterns correspond to the so-called *primary combs* where the teeth have a $L \times FSR$ separation [6, 7, 30].

The theoretical analysis of the Eckhaus instability starts with the Lugiato-Lefever equation [34], which is an accurate model to analyze the laser field dynamics in Kerr-nonlinear WGM resonators [35–37]. The slowly varying complex amplitude of the normalized intracavity field $\psi(\theta, \tau)$ obeys the equation

$$\frac{\partial \psi}{\partial \tau} = -(1 + i\alpha)\psi - i\frac{\beta}{2}\frac{\partial^2 \psi}{\partial \theta^2} + i|\psi|^2\psi + F, \qquad (1)$$
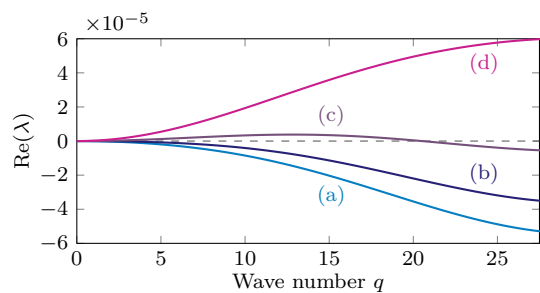

FIG. 3: (Color online) Real part of the eigenvalues of the pattern with $L = 55$ for the branch of soft modes obtained from Eq. (6). Lines (a) to (d) correspond to the parameter values indicated by blue dots in Fig. 2. The curvature of the branch progressively changes from negative to positive signaling the Eckhaus instability.

where $\theta \in [-\pi, \pi]$ is the azimuthal coordinate along the ring of the resonator, and $\tau = t/2\tau_{ph}$ is the time scaled to the photon lifetime. The normalized parameters of this equation are the continuous-wave pump field F, the frequency detuning between laser and pumped resonance frequencies α, and the group-velocity dispersion β [36].

Equation (1) has homogeneous steady states ψ_s implicitly given by $\rho_s[1 + (\rho_s - \alpha)^2] = F^2$ with $\rho_s = |\psi_s|^2$. The solution is trivalued for $\alpha > \sqrt{3}$. The line SN_b (resp. SN_t) in Fig. 2 corresponds to the saddle-node bifurcation where lower (resp. upper) and middle branches meet, so that SN_b and SN_t unfold from cusp at $\alpha = \sqrt{3}$ [6, 7]. For $\alpha < \sqrt{3}$ the solution is monovalued. In what follows we refer the lower homogeneous steady state as HSS.

In the anomalous regime ($\beta < 0$) and for $\alpha < 2$, $\rho_s = 1$ is the MI threshold above which the HSS is unstable to perturbations with wavenumber L in the neighborhood of $L_u = \sqrt{(2/\beta)(\alpha - 2\rho_s)}$ (see Fig. 2). Roll patterns with different wavenumbers can emerge although typically the one with wavenumber L_u dominates since it has the largest growth ratio. This pattern is supercritical for $\alpha < 41/30$, and sub-critical for $\alpha > 41/30$. Regarding the other possible roll patterns, it turns out that only those with wavenumber close to L_u are stable, forming what is known as a *Busse balloon* [19, 20] while the others are unstable. Moreover, in the subcritical regime, cavity solitons or localized states (LSs) coexist with the periodic patterns and the HSS. For $\alpha > 2$ the critical wavenumber is zero and the threshold $\rho_s = 1$ is a Belyakov-Devaney (BD) transition of the HSS [7, 13] (see Fig. 2).

To study the secondary bifurcations that destabilize a roll pattern of wavenumber L we perform a linear stability analysis. The stationary but θ-dependent pattern can be expanded in Fourier series

$$\psi_P(\theta) = \sum_{n=-N}^{N-1} \psi_n e^{inL\theta}, \qquad (2)$$

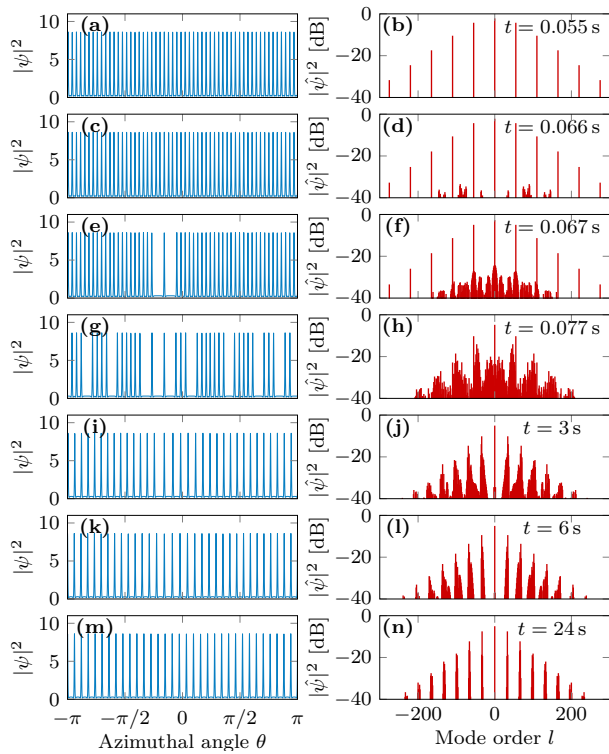with L being the integer wavenumber (or order) of the

FIG. 4: (Color online) Numerical evidence of Eckhaus instability. Nonlinear evolution of the $L = 55$ pattern after crossing the EC line as described in the main text. Left column shows the spatial profile $|\psi(\theta)|^2$ of the pattern at different times, while right column shows the corresponding power spectra $|\hat{\psi}(l)|^2$. Time stamps given in real time $t = 2\tau_{\mathrm{ph}} \times \tau = 10^{-6}\tau$. These numerical simulations show that after the Eckhaus bifurcation, the convergence towards the new pattern $L = 33$ is a very slow process that takes place in the timescale of a minute. The time needed to simulate this 24 s-long transient dynamics was about one month, using a pseudospectral algorithm where the linear terms in Fourier space are integrated exactly while the nonlinear ones are integrated using a second-order approximation in time [14].

pattern and ψ_n the complex amplitudes of the Fourier modes. We take $N = 32$ and the amplitudes can be calculated numerically by solving the stationary problem using a Newton-Raphson algorithm. Linearizing Eq. (1) about the stationary pattern $\psi_{\mathrm{P}}(\theta)$ yields the perturbation equation

$$\partial_\tau \delta\psi = -(1 + i\alpha)\delta\psi - i(\beta/2)\partial_\theta^2 \delta\psi$$
$$+2i|\psi_{\mathrm{P}}|^2\delta\psi + i\psi_{\mathrm{P}}^2\delta\psi^*. \quad (3)$$

Due to the periodicity of the system, the solution of Eq. (3) can be written as the superposition of Bloch waves

$$\delta\psi(\theta, \tau) = e^{iq\theta}\delta a(\theta, \tau, q) + e^{-iq\theta}\delta a(\theta, \tau, -q), \quad (4)$$

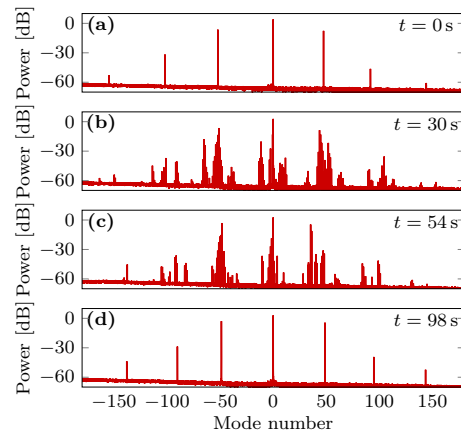where δa has the same periodicity of the pattern $\psi_{\mathrm{P}}(\theta)$,

FIG. 5: (Color online) Experimental evidence of ultra-slow Eckhaus instability around a roll patterns of wavenumber $L = 50$. The pattern becomes Eckhaus-unstable with a temporal evolution characterized by minute timescale transients, before converging towards another pattern of lower order $L = 47$.

and can be written as

$$\delta a(\theta, \tau, q) = \sum_{n=-N}^{N-1} \delta a_n(\tau, q)e^{inL\theta} \quad (5)$$

with q being an integer. Using Eq. (3), a set of linear equations for the Fourier modes $\delta a_n(\theta, q)$ can be derived [39], and in compact form they read as

$$\partial_\tau \Upsilon(\tau, q) = \mathsf{M}(\{\psi_n\}, q)\Upsilon(\tau, q), \quad (6)$$

where $\Upsilon(\tau, q) \equiv [\delta a_{-N}(\tau, q), \cdots, \delta a_{N-1}(\tau, q), \delta a_{-N}^*(\tau, -q), \cdots, \delta a_{N-1}^*(\tau, -q)]$. The stability analysis of $\psi_{\mathrm{P}}(\theta)$ reduces to find the $2N$ eigenvalues $\{\lambda_n(q)\}$ of the matrix $\mathsf{M}(\{\psi_n\}, q)$, and its corresponding eigenvectors, for each value of q. The eigenvalues for a given integer q determine the stability of the pattern against perturbations containing any set of wavenumbers $nL \pm q$. For this analysis it is sufficient to consider only the q values inside the first Brillouin zone $[0, L/2]$. We recall that $q = 0$ corresponds to the Goldstone mode associated to the translational invariance, and modes with $q \gtrsim 0$ form the branch of soft modes.

Fig. 2 shows the bifurcation lines of the roll pattern created spontaneously with the most unstable wavenumber L_{u} for $\alpha = 1$ and $F = 1.05$ ($\rho_{\mathrm{s}} = 1.095$). For the value $\beta = -8 \times 10^{-4}$ considered here, we have $L_{\mathrm{u}} = 55$. As the detuning is increased, the pattern becomes subcritical for $\alpha \simeq 41/30$, and above this value it exists between the saddle-node lines $\mathrm{SN}_{\mathrm{P}_1}$ and $\mathrm{SN}_{\mathrm{P}_2}$, although unstable below the Eckhaus line (EC). Above a certain value of the detuning and the pump, we observe a finite-wavelength Hopf (FWH) instability (dot-dashed) leading to oscillatory patterns [13, 39]. We will not consider this regime here since we focus on the Eckhaus instability. Note that pattern and HSS are stable and coexist in the parameter region limited by MI, SN_b, FWH and EC lines.

Figure 3 shows the real part of the eigenvalues of the pattern as a function of the wavenumber q for the branch of soft modes [39]. The parameters correspond to those of the blue dots in Fig. 2, while crossing the Eckhaus instability. The change of convexity of the branch at $q = 0$ is what precisely signals the Eckhaus instability. After the instability, the pattern becomes unstable to small-wavenumber perturbations. Well beyond the instability, the mode with maximum growth rate has a wavenumber close to the edge of the Brillouin zone $q = L/2$.

After encountering an Eckhaus instability a pattern with a wavenumber which is too large to be stable looses cells in such a way that the new wavenumber lies in the stability balloon [15]. For supercritical patterns this happens at a relatively fast time scale. For subcritical patterns, the HSS is stable and coexists with the pattern allowing the formation of LS. When a cell is lost the space is occupied by the HSS leading to a transient state formed by groups of LSs separated by the HSS, known as cracking pattern [38]. If LSs have oscillatory tails they may lock at specific distances given by multiples of the oscillatory tail wavelength, thus the cracking pattern is stationary. On the contrary, if LS tails are monotonous, LS repel each other and the cracking pattern evolves towards a periodic solution with equally spaced peaks and a stable wavenumber. In practice, a similar behavior is observed if tails are oscillatory with a wavelength much larger than the typical separation between peaks. This transient behavior can be extremely slow as the interaction decays exponentially with the distance between peaks allowing for long-lived cracking patterns likely to be observed at second- and even minute-timescale in experiments.

In our numerical simulations, the Eckhaus instability is triggered by slowly ramping up the detuning and the pump parameter. This procedure is consistent with the experimental system where the detuning is thermally driven across the resonance [40]. The dotted line in Fig. 2 shows the ramp of parameter values used in the simulation shown in Fig. 4. The simulation starts at $t = 0$ with $\alpha = 1$ and $F = 1.05$, just above the MI, and a stable pattern with $L = 55$ emerges, corresponding to the wavenumber with maximum growth rate L_u. The parameters are ramped until $t = 0.05$ s with $\alpha = 3.8$ and $F = 2$, above the Eckhaus instability. The simulation then continues up to $t = 24$ s (which corresponds to 24 million photon lifetimes in our resonator), with clamped values for θ and F. The original pattern, whose spatial profile and power spectrum is shown Figs. 4(a) and (b), remains stable through the ramp until it crosses the EC line. At this point the pattern becomes unstable and soft mode perturbations start to grow. As a consequence some pattern cells disappear as shown in Figs. 4(c) and (d). Further development of the instability leads to a cracked pattern as shown in Figs. 4(e) and (f) for time $t = 0.077$ s. For the parameters considered, LSs have oscillatory tails although the wavelength of the tail oscillations is much larger than the separation between consecutive peaks [41]. As a consequence, LSs do not get pinned, but they repel each other instead. This ultra-slow dynamics can take more than a minute to converge asymptotically to another pattern, as observed experimentally in Fig. 5. In contrast for all nonlinear effects reported so far using the LLE, the transient dynamics usually last only few τ_{ph} (i. e., few µs in our case). Note that if the ramp is increased to much larger values of the detuning, one reaches the single-soliton regime described in [43] and eventually only a single peak survives.

Figure 5 shows an experimental example of primary comb of order corresponding to a high-wavenumber roll patterns with $L = 50$. When the laser frequency is thermally driven across from the resonance, we observe the emergence of spurious peaks around the main primary comb, and the comb dynamics is characterized by a very slow timescale, that can be larger than a minute. This timescale appears *a priori* as inconsistent with the intrinsic Kerr comb dynamics, where the slowest timescale is generally the photon lifetime $\tau_{\mathrm{ph}} = Q/\omega_0 \sim 1$ µs, with $Q \sim 10^9$ being the loaded quality factor of our resonator and ω_0 is the angular frequency of the pumped mode [31–33]. However, as demonstrated earlier, a detailed analysis unveils that the mechanism behind this ultra-slow timescale dynamics is an Eckhaus instability leading to very-long-lasting transient cracking patterns, and later on to a lower order stable roll pattern.

In conclusion, we have experimentally evidenced Eckhaus instability in a whispering-gallery mode resonator. The emerging timescale of the instability, dominated by the interaction between LSs, was shown to be six to eight orders of magnitude larger than the intracavity photon lifetime, which is the natural timescale for Kerr comb dynamics. These results permit to achieve a deeper understanding of secondary bifurcations in dissipative optical systems, and future work will investigate in detail the wide variety of spatiotemporal patterns that can be excited via these bifurcations, including when co-induced by other bulk nonlinearities [4, 44, 45].

* damia@ifisc.uib-csic.es

† ykchembo@umd.edu

[1] P. Del'Haye, A. Schliesser, O. Arcizet, T. Wilken, R. Holzwarth, and T. J. Kippenberg, Optical frequency comb generation from a monolithic microresonator, Nature **450**, 1214 (2007).

[2] T. J. Kippenberg, R. Holzwarth, and S. A. Diddams, Microresonator-Based Optical Frequency Combs, Science **332**, 555 (2011).

[3] Y. K. Chembo, Kerr optical frequency combs: theory, applications and perspectives, Nanophotonics **5**, 214 (2016).

[4] G. Lin, A. Coillet and Y. K. Chembo, Nonlinear photonics with high-Q whispering-gallery-mode resonators, Adv. Opt. Phot. **9**, 828 (2017).

[5] A. Pasquazi, M. Peccianti, L. Razzari, D. J. Moss, S. Coen, M. Erkintalo, Y. K. Chembo, T. Hansson, S. Wabnitz, P. Del'Haye, X. Xue, A. M. Weiner, and R. Morandotti, Micro-combs: A novel generation of optical sources, Phys. Rep. **729**, 1 (2018).

[6] C. Godey, I. V. Balakireva, A. Coillet and Y. K. Chembo, Stability analysis of the spatiotemporal Lugiato-Lefever model for Kerr optical frequency combs in the anomalous and normal dispersion regimes, Phys. Rev. A **89**, 063814 (2014).

[7] P. Parra-Rivas, D. Gomila, M. A. Matias, S. Coen, and L. Gelens, Dynamics of localized and patterned structures in the Lugiato-Lefever equation determine the stability and shape of optical frequency combs, Phys. Rev. A **89**, 043813 (2014).

[8] P. Parra-Rivas, E. Knobloch, D. Gomila and L. Gelens, Dark solitons in the Lugiato-Lefever equation with normal dispersion, Phys. Rev. A **93**, 063839 (2016).

[9] C. Godey, A bifurcation analysis for the Lugiato-Lefever equation, Eur. Phys. J. D **71** 131 (2017).

[10] L. Delcey and M. Haragus, Periodic waves of the Lugiato-Lefever equation at the onset of Turing instability, Phil. Trans. R. Soc. A **376**, 20170188 (2018).

[11] F. Leo, L. Gelens, P. Emplit, M. Haelterman, and S. Coen, Dynamics of one-dimensional kerr cavity solitons, Opt. Express **21**, 9180 (2013).

[12] P. Parra-Rivas, D. Gomila, L. Gelens, and E. Knobloch, Bifurcation structure of localized states in the Lugiato-Lefever equation with anomalous dispersion, Phys. Rev. E **97**, 042204 (2018).

[13] P. Parra-Rivas, D. Gomila, L. Gelens, and E. Knobloch, Bifurcation structure of periodic patterns in the Lugiato-Lefever equation with anomalous dispersion, Phys. Rev. E **98**, 042212 (2018).

[14] The asymptotic numerical error is a numerical noise floor that is independent of the length of the simulation, since we are simulating the convergence of a system towards a stable fixed point (attractor) in the state space.

[15] N. Périnet, N. Verschueren, and S Coulibaly, Eckhaus instability in the Lugiato-Lefever model, Eur. Phys. J. D. **71**, 243 (2017).

[16] Z. Liu, F. Leo, S. Coulibaly, and M. Taki, Secondary instabilities in all fiber ring cavities, Phys. Rev. A **90**, 033837 (2014).

[17] S. Coulibaly, M. Taki, A. Bendahmane, G. Millot, B. Kibler, and M. G. Clerc, Turbulence-induced rogue waves in Kerr resonators, Phys. Rev. X **9**, 011054 (2019).

[18] W. Eckhaus, *Studies in Nonlinear Stability Theory* (Springer, New York, 1965).

[19] D. Walgraef, *Spatio-Temporal Pattern Formation* (Springer, New York, 1997).

[20] M. Cross and H. Greenside, *Pattern Formation and Dynamics in Nonequilibrium Systems* (Cambridge University Press, Cambridge, 2009).

[21] L. S. Tuckerman and D. Barkley, Bifurcation analysis of the Eckhaus instability, Physica D **46D**, 57 (1990).

[22] G. Ahlers, D. S. Cannell, M. A. Dominguez-Lerma, and R. Heinrichs, Wavenumber selection and Eckhaus instability in Couette-Taylor flow, Physica D **23**, 202 (1986).

[23] M. Lowe and J. P. Gollub, Pattern Selection near the Onset of Convection: The Eckhaus Instability, Phys. Rev. Lett. **55**, 2575 (1985).

[24] E. Louvergneaux, Pattern-Dislocation-Type Dynamical Instability in 1D Optical Feedback Kerr Media with Gaussian Transverse Pumping, Phys. Rev. Lett. **87**, 244501 (2001).

[25] J. Plumecoq, C. Szwaj, D. Derozier, M. Lefranc, and S. Bielawski, Eckhaus instability induced by nonuniformities in a laser, Phys. Rev. A **64**, 061801(R) (2001).

[26] F. Li, K. Nakkeeran, J. N. Kutz, J. Yan, Z. Kang, X. Zhang, and P. K. A. Wai, Eckhaus Instability in the Fourier-Domain Mode Locked Fiber Laser Cavity, arXiv: 1707.08304v1 (2017).

[27] M. Wolfrum and S. Yanchuk, Eckhaus Instability in Systems with Large Delay, Phys. Rev. Lett. **96**, 220201 (2006).

[28] H. Riecke and H. G. Paap, Perfect Wave-Number Selection and Drifting Patterns in Ramped Taylor Vortex Flow, Phys. Rev. Lett. **59**, 2570 (1987).

[29] G. Lin and Y. K. Chembo, On the dispersion management of fluorite whispering-gallery mode resonators for Kerr optical frequency comb generation in the telecom and mid-infrared range, Optics Express **23**, 1594 (2015).

[30] K. Saleh and Y. K. Chembo, On the phase noise performance of microwave and millimeter-wave signals generated with versatile Kerr optical frequency combs, Opt. Express **24**, 25043 (2016).

[31] Y. K. Chembo and N. Yu, On the generation of octave-spanning optical frequency combs using monolithic whispering-gallery-mode microresonators, Opt. Lett. **35**, 2696 (2010).

[32] A. Coillet, R. Henriet, K.-P. Huy, M. Jacquot, L. Furfaro, I. Balakireva, L. Larger and Y. K. Chembo, Microwave photonics systems based on whispering-gallery-mode resonators, J. Vis. Exp. **78**, e50423 (2013).

[33] R. Henriet, G. Lin, A. Coillet, M. Jacquot, L. Furfaro, L. Larger and Y. K. Chembo, Kerr optical frequency comb generation in strontium fluoride whispering-gallery mode resonators with billion quality factor, Opt. Lett. **40**, 1567 (2015).

[34] L. A. Lugiato and R. Lefever, Spatial Dissipative Structures in Passive Optical Systems, Phys. Rev. Lett. **58**, 2209 (1987).

[35] A. B. Matsko, A. A. Savchenkov, W. Liang, V. S. Ilchenko, D. Seidel, and L. Maleki, Mode-locked Kerr frequency combs, Opt. Lett. **36**, 2845 (2011).

[36] Y. K. Chembo and C. R. Menyuk, Spatiotemporal Lugiato-Lefever formalism for Kerr-comb generation in whispering-gallery-mode resonators, Phys. Rev. A **87**, 053852 (2013).

[37] S. Coen, H. G. Randle, T. Sylvestre, and M. Erkintalo, Modeling of octave-spanning Kerr frequency combs using a generalized mean-field Lugiato-Lefever model, Opt. Lett. **38**, 37 (2013).

[38] G. K. Harkness, W. J. Firth, G.-L. Oppo, and J. M. McSloy, Computationally determined existence and stability of transverse structures. I. Periodic optical patterns, Phys. Rev. E **66**, 046605 (2002).

[39] D. Gomila and P. Colet, Dynamics of hexagonal patterns in a self-focusing Kerr cavity, Phys. Rev. E **76**, 016217 (2007).

[40] S. Diallo, G. Lin and Y. K. Chembo, Giant thermo-optical relaxation oscillations in millimeter-size whispering gallery mode disk resonators, Opt. Lett. **40**, 3834 (2015).

[41] The wavelength of the spatial oscillations in the tails of the LS calculated from the imaginary part of the spatial eigenvalues of the HSS [42] for the parameters used in the simulations is $\pi/6.59$, larger than the typical separation between peaks.

[42] P. Parra-Rivas, D. Gomila, P. Colet, and L. Gelens, Interaction of solitons and the formation of bound states in the generalized Lugiato-Lefever equation, Eur. Phys. J. D **71**, 198 (2017).

[43] T. Herr, V. Brasch, J. D. Jost, C. Y. Wang, N. M. Kondratiev, M. L. Gorodetsky, and T. J. Kippenberg, Temporal solitons in optical microresonators, Nature Photon. **8**, 145 (2014).

[44] G. Lin and Y. K. Chembo, Phase-locking transition in Raman combs generated with whispering gallery mode resonators, Opt. Lett. **41**, 3718 (2016).

[45] G. Lin, S. Diallo, J. M. Dudley and Y. K. Chembo, Universal nonlinear scattering in ultra-high) Q whispering-gallery mode resonators, Opt. Express **24**, 14880 (2016).